chondroitinase (CSase) B and a mixture of CSases AC-I and AC-II (CSase AC), respectively. CSase B cleaves the *N*-acetyl-D-galactosaminidic linkage in the GalNAc(4S)-L-iduronic acid (IdoUA) (±2S) sequences and yields unsaturated disaccharides, ΔHexUA (4,5-unsaturated hexuronic acid)-GalNAc(4S) and ΔHexUA(2S)-GalNAc (4S) [Sugahara and Mikami, 2007; Yoshida et al., 1993], where 2S and 4S represent 2-*O*-sulfate and 4-*O*-sulfate, respectively. The 4-*O*-sulfation of GalNAc residues is essential for recognition by CSase B. In contrast, CSase AC does not act on IdoUA-containing sequences but degrades the *N*-acetyl-D-galactosaminidic linkages in the GalNAc (±4S, ±6S)-D-glucuronic acid (GlcUA) sequences [Linhardt et al., 2006], where 6S stands for 6-*O*-sulfate. When digested with CSase B, 4-*O*-sulfated unsaturated disaccharides were detected only in the controls but not in the patients (Fig. 2D and Supp. Table S1), suggesting that D4ST1 is the major enzyme for 4-*O*-sulfation of DS in normal human skin fibroblasts and cannot be compensated functionally either by chondroitin 4-*O*-sulfotransferase 1 or 2.

To investigate whether the loss-of-function mutations in D4ST1 lead to an increase in nonsulfated dermatan, the GAG fraction prepared from the fibroblasts of the patients and controls were digested with CSase ABC, which cleaves all the *N*-acetyl-D-galactosaminidic linkages in CS/DS chains including the non-sulfated GalNAc-IdoUA sequence that is resistant to CSase B [Yoshida et al., 1993]. Notably, the proportion of the non-sulfated disaccharide ΔHexUA-GalNAc in the patients was very low (Supp. Table S1), suggesting that nonsulfated dermatan was negligible. Conversion of GlcUA to IdoUA most likely occurs even in the patients. However, the epimerization reaction is reversible that favors the GlcUA formation, and D4ST1 probably functions as the "4-*O*-sulfation lock" of IdoA [Malmström, 1984]. Hence, the defect in D4ST1 probably allowed back epimerization reactions converting IdoUA to GlcUA to form CS in the patients. The total amount of CS/DS disaccharides did not show a significant difference between the patients and controls (Fig. 2E). CS disaccharides produced by digestion with CSase AC increased markedly in the cell lysates of fibroblasts from the patients compared with those from the controls, suggesting the upregulation of CS chain biosynthesis (diverted from DS) in the patients.

Glycosaminoglycan of Decorin

We then examined decorin as a major DS proteoglycan in skin. Decorin directly binds to collagen via its core protein and the GAG side chains aggregate and function as interfibrillar bridges [Scott, 1996, 2003]. Decorin purified from the fibroblasts of the patients was resistant to CSase B, indicating that its GAG side chain consisted of only CS but no DS disaccharides, while decorin in the controls contained a hybrid CS/DS chain (Fig. 3A). Actually, the GAG side chain of decorin from the controls was mainly composed of DS disaccharides (approximately 95%), IdoUA-GalNAc(4S), and IdoUA(2S)-GalNAc(4S), but contained a small portion of CS disaccharide, GlcUA-GalNAc(4S) (Fig. 3B). In contrast, no DS disaccharides were detected in the decorin proteoglycan from the patients (Fig. 3B). Its GAG side chain most likely consisted of only CS disaccharides including 4-*O*-sulfated and 6-*O*-sulfated disaccharide units. These data and those shown in Figure 2E suggest that the DS chain of decorin proteoglycan in the patients has been replaced by CS.

TGF-β Signaling Is Unaltered in Fibroblasts Derived from Patients

DS proteoglycan is known to be related to TGF-β signaling [Hocking et al., 1998; Tiedemann et al., 2005; Yamaguchi et al., 1990]. As decorin neutralizes TGF-β1 activity [Yamaguchi et al., 1990], we examined whether *CHST14* aberrations would affect TGF-β1 signal transduction. We overexpressed wild-type or mutant *CHST14* cDNA in the fibroblasts from patients in which endogenous *CHST14* expression was negligible and found that the levels of *CHST14* expression from transgenes were approximately 300-fold those of endogenous mutant *CHST14* expression at 56 hr after transfection (Supp. Fig. S2A). To investigate whether *CHST14* overexpression would affect TGF-β signaling in the patient fibroblasts, we performed three different experiments. First, we measured the expression of *PAI1* and *SMAD7*, which are direct downstream targets of TGF-β. The expression of *PAI1* and *SMAD7* was significantly upregulated at 24 hr after TGF-β1 treatment. However, the degree of upregulation was not different between the cells transfected with empty or *CHST14* expression

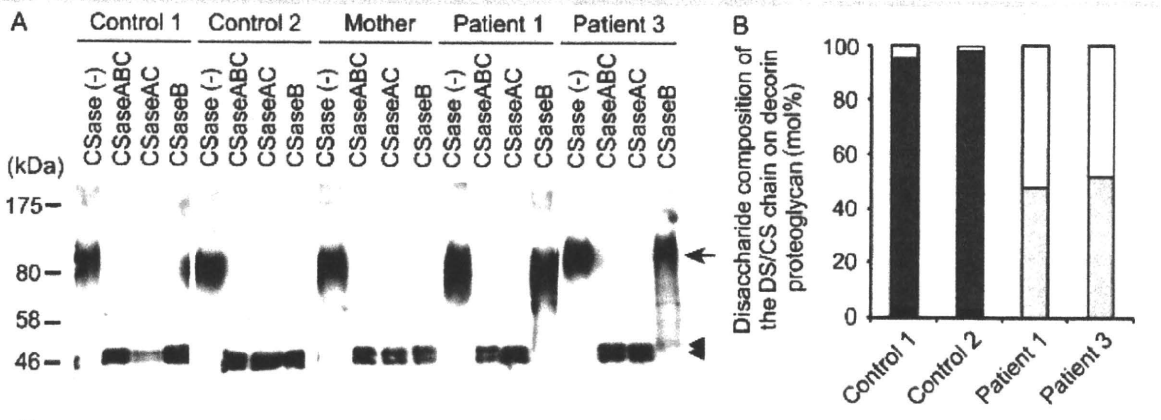

Figure 3. Disaccharide composition analysis of CS/DS chains of decorin. **A:** Immunoblot of decorin proteoglycans. Each serum-free conditioned medium of skin fibroblasts was digested with CSase ABC, CSase AC, CSase B, or buffer alone (−) and then subjected to Western blotting using an antihuman decorin antibody. The arrow and arrowheads indicate the decorin proteoglycans and the core protein of decorin without a CS/DS side chain, respectively. **B:** Proportion of the disaccharide units in the CS/DS hybrid chain in decorin proteoglycans secreted by the fibroblasts. White, light gray, dark gray, and black boxes are GlcUA-GalNAc(4S), GlcUA-GalNAc(6S), IdoUA-GalNAc(4S), and IdoUA(2S)-GalNAc(4S), respectively.

vectors (Supp. Fig. S2B). Second, TGF-β1 transmits signals to the nucleus via phosphorylation of SMAD2/3 proteins. Therefore, a reporter gene assay was performed using SBE4-luc vector, a TGF-β-responsive reporter containing four tandem copies of the SMAD-binding element (SBE). *CHST14* overexpression did not affect the reporter activity upregulated by TGF-β1 treatment (Supp. Fig. S2C). Third, we examined the level of phosphorylated SMAD2 proteins by Western blot analysis. Although TGF-β1 treatment clearly stimulated the phosphorylation of SMAD2, there were no significant differences between the cells transfected with empty or *CHST14* vectors (Supp. Fig. S2D). The same results from these three experiments were obtained using fibroblasts from another patient (data not shown). Furthermore, we confirmed that overexpression of the mutant D4ST1 enzymes identified in patients did not affect TGF-β signaling in normal fibroblasts (data not shown). These results imply that TGF-β signaling might not be changed in the fibroblasts from patients with a D4ST1 deficit.

Histopathological Examination

Hematoxylin and eosin (H&E)-stained light microscopy on patients' skin specimens showed that fine collagen fibers were predominant in the reticular to papillary dermis and normally thick collagen bundles were markedly reduced (Fig. 4). Electron microscopy showed that the collagen fibrils were dispersed in the reticular dermis, compared with regularly and tightly assembled ones observed in the control, whereas each collagen fibril was smooth and round, not varying in size and shape, similar to each fibril of the control (Fig. 4).

Discussion

In this study, we identified a total four *CHST14* mutations (three missense and one nonsense) in six Japanese patients presenting with a new type of EDS [Kosho et al., 2010]. This disorder represents all hallmarks of EDS: skin hyperextensibility, joint hypermobility, and tissue fragility affecting skin, ligaments, joints, blood vessels, and internal organs [Steinmann et al., 2002]. Tentatively we categorized patients 1 and 2 before as EDS VIB, a subtype of kyphoscoliosis type without lysyl hydroxylase deficiency, based on cutaneous (hyperextensibility, bruisability, fragility with atrophic scars) and skeletal (generalized joint laxity, kyphoscoliosis, Marfanoid habitus) features as well as mild delay of motor development with hypotonia in infancy [Kosho et al.,

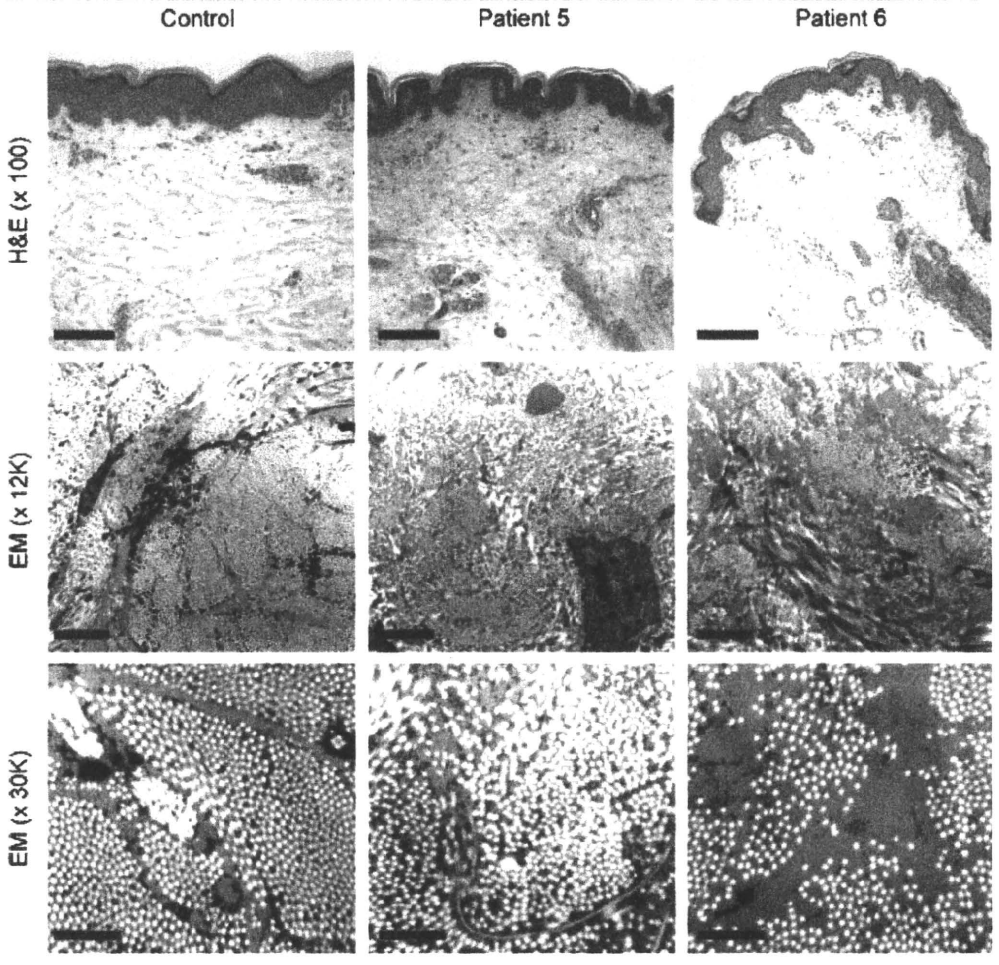

Figure 4. Pathological examination of dermal tissues from patients. H&E-stained light microscopy (upper picture) on skin specimens of patients 5 and 6 (× 100) shows that fine collagen fibers were present predominantly in the reticular to papillary dermis with marked reduction of normally thick collagen bundles. Electron microscopy (EM) (× 12,000 middle picture; × 30,000 lower picture) showed that collagen fibrils were dispersed in the reticular dermis, compared with the regularly and tightly assembled ones observed in the control subject. However, each collagen fibril was smooth and round, not varying in size, similar to the control. Scale bars indicate 500 μm (upper picture), 2 μm (middle), and 1 μm (lower).

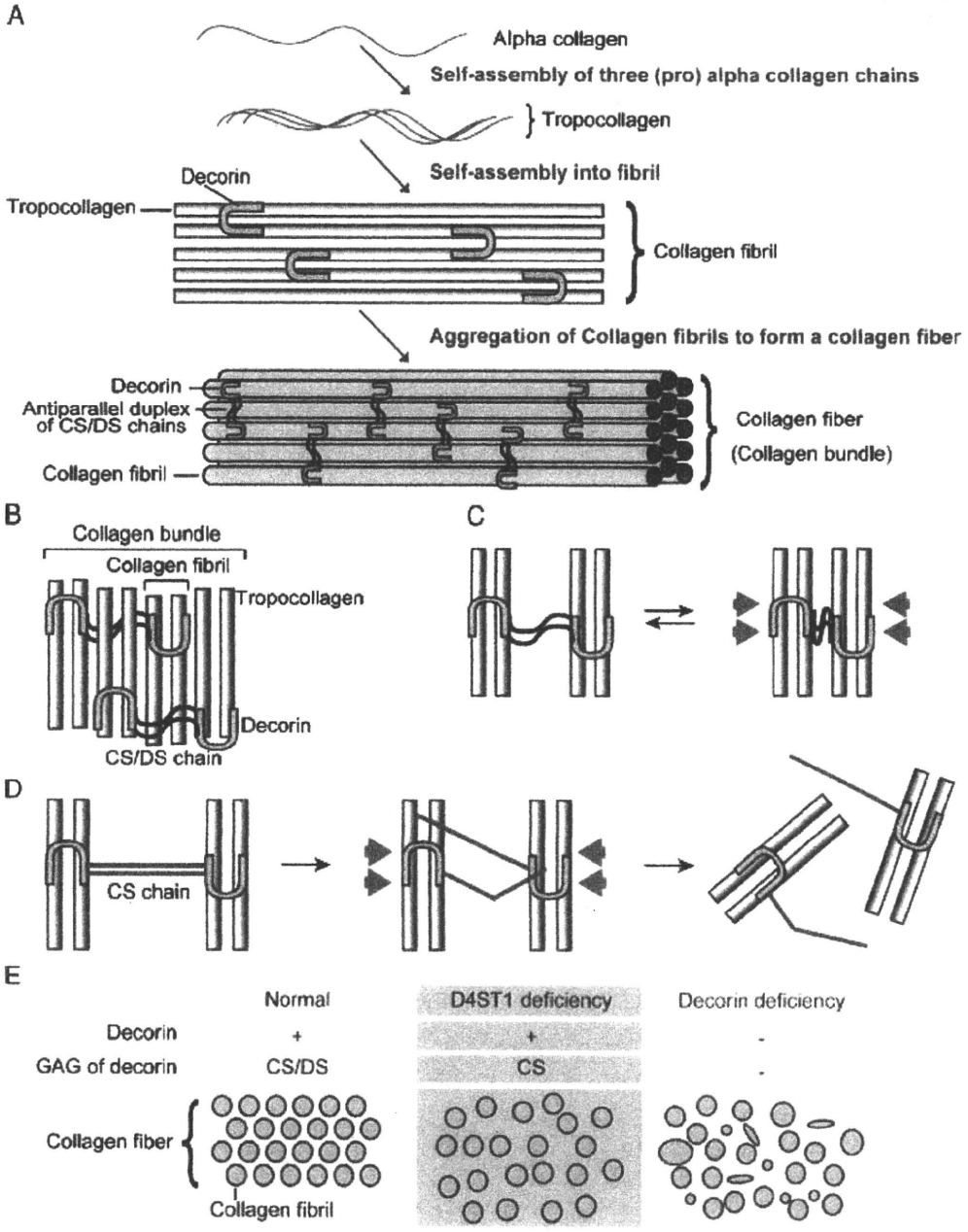

Figure 5. Putative model for abnormal collagen bundle assembly in this disease. **A:** The scheme of the collagen biosynthesis. Three alpha collagen chains are self-assembled into form a tropocollagen unit. Tropocollagens are packed via decorin to form a collagen fibril. Decorin core protein directly binds to collagen's particular amino sequence. Collagen fibrils assemble to form the collagen fiber, also called a collagen bundle when thick. **B:** The relationship between collagen fibril and decorin proteoglycan. Collagen fibrils are assembled into a collagen bundle by the antiparallel complex of the CS/DS hybrid GAG chains of decorin proteoglycan like a bridge to keep the space between fibrils and make collagen fiber tighter. **C, D:** The structural alteration of collagen fibers by mechanical compression in normal and affected states, respectively. CS/DS hybrid chains are able to bend against mechanical compression and rebound to form the original structure, because GAG chains function as suspension (C). D4ST1 defects result in absence of CS/DS hybrid chains in decorin (D). Replaced CS chains might not form collagen bundles properly. Even if they can form bundles, decorin CS chains cannot resist mechanical stresses and collagen fibrils get scattered after repetitive stresses irreversibly, as observed in patients (D). Red arrows indicate mechanical pressures. **E:** Comparisons of collagen fiber formation in normal (left), D4ST1 deficiency (middle), and decorin (core protein) deficiency (right). Collagen fibrils normally aggregate in line and form collagen fibers. The fibrils are round and uniform. In D4ST1 deficiency, collagen fibrils are scattered, although the shape and size of collagen fibrils are unchanged. Irregular shapes and sizes of collagen fibrils were seen in decorin null mice [Danielson et al., 1997], being apparently different from those in D4ST1 deficiency.

2005]. Patients in our series [Kosho et al., 2010] shared many clinical features with a Pakistani sister and brother reported by Steinmann et al. [1975], including down-slanting palpebral fissures, high palate, talipes equinovarus, progressive talipes vagus and planus, joint laxity, scoliosis, skin hyperextensibility, bruisability, and fragility with atrophic scars; hyperalgesia to pressure,

radiologically identified tall vertebral bodies and diaphysial narrowing of phalanges, metacarpals, and metatarsals; and delayed motor development. The sibs have been classified into EDS VIB [Steinmann et al., 2002], with the lysyl hydroxylase activity proved to be normal [Wenstrup et al., 1989]. Pathological findings were similar to those observed in our series: light microscopically, collagen bundles were interspersed with filamentous material that stained only faintly; and, electron microscopically, a great proportion of collagen fibrils was not integrated into bundles but dispersed into the ground substance [Steinmann et al., 1975].

CHST14 has recently been demonstrated as the causative gene for adducted thumb–clubfoot syndrome (ATCS; MIM# 601776), another autosomal recessive disorder [Dündar et al., 2009]. ATCS has been categorized as a new type of arthrogryposis, based on characteristic clinical pictures from birth to early childhood, including adducted thumbs and clubfoot as well as craniofacial dysmorphism (broad or bossed forehead, brachycephaly, late-closing large fontanelle, hypertelorism, downslanting palpebral fissures, blue sclerae, low-set posteriorly rotated or dysplastic ears, high or cleft palate, short neck), arachnodactyly with tapering fingers, cryptorchidism, inguinal hernia, atrial septal defect, kidney defects, cranial ventricular enlargement, and psychomotor retardation [Dündar et al., 1997, 2001; Janecke et al., 2001; Sonoda and Kouno, 2000]. In a recent study by Dündar et al. [2009], ATCS has been again categorized as a connective tissue disorder, based on additional clinical pictures from childhood to adolescence, including skin fragility, bruisability, and translucency; joint laxity, and osteopenia. In 11 ATCS patients from four families identified to date [Dündar et al., 2009], 5 died in early infancy or childhood: a male from a Austrian family (p.R213P) died shortly after birth due to respiratory failure [Janecke et al., 2001]; a female from a Turkish family (p.V49X) died at age 6 years [Dündar et al., 1997], and a female and two males from a Turkish family (p.[R135G]+[L137Q]) died before 4 months of age [Dündar et al., 2001]. ATCS patients may have wider and more severe manifestations than our series, implicating roles for DS not only in connective tissue maintenance but also in embryonic development [Dündar et al., 2009]. Furthermore, a skin specimen from a patient was interpreted as showing normal structure and ultrastructure [Dündar et al., 2009]. To date, it would be difficult to delineate whether a new type of EDS we have proposed and ATCS would be distinct clinical entities or a single clinical entity (D4ST1 deficiency) with variable inter- and intrafamilial expressions and with different presentations depending on the patients' ages at diagnosis. Longitudinal clinical information of ATCS patients would solve this issue.

Collagen bundles are composed of many collagen fibrils linked via antiparallel CS/DS chain complexes (Fig. 5A and B). The property of reversible deformation of proteoglycan comes from antiparallel anionic GAG chain formation [Scott, 2003]. Interestingly, the structure of DS chains is flexible, whereas that of CS chains is rigid, because L-IdoUA residues in DS can switch readily between almost equi-energetic $^{1}C_{4}$, $^{2}S_{0}$, and $^{4}C_{1}$ conformers; by comparison GlcUA in CS adopts purely the $^{4}C_{1}$ conformation [Casu et al., 1988; Catlow et al., 2008]. Transition from the CS/DS hybrid chain of decorin to a CS chain probably decreases the flexibility of the GAG chain and break the GAG antiparallel complex after compression stresses (Fig. 5C and D). This irreversible event could explain the progressive course of this disease. In the patients, the size and shape of the collagen fibrils seemed normal, whereas the collagen bundles were not properly organized. In decorin null mice, dermal collagen fibrils showed huge varieties of size and shape [Danielson et al., 1997]. These findings suggest that the core protein of decorin is important for collagen fibril formation, and that the CS/DS hybrid chain of decorin proteoglycan regulates the space between the collagen fibrils and forms collagen bundles as reported previously (Fig. 5E) [Scott, 1995]. Decorin is able to neutralize the growth-stimulatory activity of TGF-β1 in Chinese hamster ovary cells through the interaction of TGF-β1 with decorin via its core protein, not via a GAG chain [Yamaguchi et al., 1990]. In our transfection experiments with *CHST14* cDNAs, no significant effects on TGF-β signaling between wild-type and mutants were detected, implying the importance of the decorin core protein (not GAG) for TGF-β signaling (Supp. Fig. S2).

In conclusion, we have detected *CHST14* mutations causing a new type of EDS with distinct craniofacial characteristics, multiple congenital contractures, progressive joint and skin laxity, and multisystem fragility related manifestations. Abnormal collagen bundle formation would be a main pathology associated with a decorin GAG abnormality. Decorin GAG side chains in the patients consist of only CS but no DS disaccharides. CS/DS hybrid chains are more flexible than CS chains. Collagen bundles bound by CS chains instead of CS/DS chains in patients should be more fragile than those in controls. These findings underscore the important aspects of decorin proteoglycans in the extracellular matrix and provide new insights for human connective tissue disorders.

Acknowledgments

We thank all the patients and their families for participating in this work. We also thank Ms. Y. Yamashita, Ms. T. Taniguchi, and Dr. S. Tominaga for their technical assistance, Drs. Y. Igawa, T. Miyahara (Shinshu University School of Medicine), Y. Seta, Y. Toki, K. Ono, T. Kosuda, A. Inoue (Tomioka General Hospital, Tomioka), T. Miyamoto (Meido Eye Clinic), K. Arai (Komachi Clinic), T. Shimizu (Gunma Spine Center), F. Miura, H. Ikei (Saku Central Hospital), N. Hoshino (Minami-Aiki-Mura Clinic), T. Muneta (Tokyo Medical and Dental University), N. Kurosawa (Tsuchiura Kyodo General Hospital), M. Nagasaka, M. Kato (Aichi Prefectural Colony Central Hospital), M. Kohyama (JA Hiroshima General Hospital), and T. Hattori (Aichi Children's Health and Medical Center) for providing clinical information of the patients. Dr. A. Kosaku (Dokkyo Medical University) kindly performed the electron microscopy. Grant sponsor: the Ministry of Education, Culture, Sports, Science and Technology; grant numbers: 21790341 (to N. Miyake), B-20390019 (to K.S.) and A-21249024 (to N. Matsumoto). Grant sponsor: the Japan Science and Technology Agency; grant number: 2014 (to N. Matsumoto). Grant sponsor: the Ministry of Health, Labour and Welfare, Japan; grant numbers: 2141039040 (to T.K. and N. Matsumoto), 20-S-3 (to S.I.). Grant sponsors: the Shinshu Association for the Advancement of Medical Sciences (to T.K.); a Grant-in-Aid for Exploratory Research of Young Scientists, Shinshu University (to T.K.); the Takeda Science Foundation (to N. Miyake); the Yokohama Foundation for Advancement of Medical Science; grant number: W2105 (to N. Miyake). Grant sponsor: the Hayashi Memorial Foundation for Female Natural Scientists; grant number: 09R198 (to N. Miyake). Grant sponsor: the Human Frontier Science Program; grant number; RGP0018/2005-C (to K.S.). This work has been done at Advanced Medical Research Center, Yokohama City University.

References

Beighton P, De Paepe A, Steinmann B, Tsipouras P, Wenstrup RJ. 1998. Ehlers-Danlos syndromes: revised nosology, Villefranche, 1997. Ehlers-Danlos National Foundation (USA) and Ehlers-Danlos Support Group (UK). Am J Med Genet 77:31–37.

Casu B, Petitou M, Provasoli M, Sinay P. 1988. Conformational flexibility: a new concept for explaining binding and biological properties of iduronic acid-containing glycosaminoglycans. Trends Biochem Sci 13:221–225.

Catlow KR, Deakin JA, Wei Z, Delehedde M, Fernig DG, Gherardi E, Gallagher JT, Pavao MS, Lyon M. 2008. Interactions of hepatocyte growth factor/scatter factor with various glycosaminoglycans reveal an important interplay between the presence of iduronate and sulfate density. J Biol Chem 283:5235–5248.

Danielson KG, Baribault H, Holmes DF, Graham H, Kadler KE, Iozzo RV. 1997. Targeted disruption of decorin leads to abnormal collagen fibril morphology and skin fragility. J Cell Biol 136:729–743.

Dündar M, Demiryilmaz F, Demiryilmaz I, Kumandas S, Erkilic K, Kendirci M, Tuncel M, Ozyazgan I, Tolmie JL. 1997. An autosomal recessive adducted thumb-club foot syndrome observed in Turkish cousins. Clin Genet 51:61–64.

Dündar M, Kurtoglu S, Elmas B, Demiryilmaz F, Candemir Z, Ozkul Y, Durak AC. 2001. A case with adducted thumb and club foot syndrome. Clin Dysmorphol 10:291–293.

Dündar M, Muller T, Zhang Q, Pan J, Steinmann B, Vodopiutz J, Gruber R, Sonoda T, Krabichler B, Utermann G, Baenziger JU. 2009. Loss of dermatan-4-sulfotransferase 1 function results in adducted thumb-clubfoot syndrome. Am J Hum Genet 85:873–882.

Hiyama K, Okada S. 1975. Amino acid composition and physiochemical characterization of chondroitinase from *Arthrobacter aurescens*. J Biochem 78:1183–1190.

Hocking AM, Shinomura T, McQuillan DJ. 1998. Leucine-rich repeat glycoproteins of the extracellular matrix. Matrix Biol 17:1–19.

Janecke AR, Unsinn K, Kreczy A, Baldissera I, Gassner I, Neu N, Utermann G, Muller T. 2001. Adducted thumb-club foot syndrome in sibs of a consanguineous Austrian family. J Med Genet 38:265–269.

Kinoshita A, Sugahara K. 1999. Microanalysis of glycosaminoglycan-derived oligosaccharides labeled with a fluorophore 2-aminobenzamide by high-performance liquid chromatography: application to disaccharide composition analysis and exosequencing of oligosaccharides. Anal Biochem 269:367–378.

Kosho T, Miyake N, Hatamochi A, Takahashi J, Kato H, Miyahara T, Igawa Y, Yasui H, Ishida T, Ono K, Kosuda T, Inoue A, Kohyama M, Hattori T, Ohashi H, Nishimura G, Kawamura R, Wakui K, Fukushima Y, Matsumoto N. 2010. A new Ehlers-Danlos Syndrome with craniofacial characteristics, multiple congenital contractures, progressive joint and skin laxity, and multisystem fragility-related manifestations. Am J Med Genet A [Epub ahead of print].

Kosho T, Takahashi J, Ohashi H, Nishimura G, Kato H, Fukushima Y. 2005. Ehlers-Danlos syndrome type VIB with characteristic facies, decreased curvatures of the spinal column, and joint contractures in two unrelated girls. Am J Med Genet A 138A:282–287.

Linhardt RJ, Avci FY, Toida T, Kim YS, Cygler M. 2006. CS lyases: structure, activity, and applications in analysis and the treatment of diseases. Adv Pharmacol 53:187–215.

Malmström A. 1984. Biosynthesis of dermatan sulfate. II. Substrate specificity of the C-5 uronosyl epimerase. J Biol Chem 259:161–165.

Mao JR, Bristow J. 2001. The Ehlers-Danlos syndrome: on beyond collagens. J Clin Invest 107:1063–1069.

Michelacci YM, Dietrich CP. 1974. Isolation and partial characterization of an induced chondroitinase B from *Flavobacterium heparinum*. Biochem Biophys Res Commun 56:973–980.

Mikami T, Mizumoto S, Kago N, Kitagawa H, Sugahara K. 2003. Specificities of three distinct human chondroitin/dermatan N-acetylgalactosamine 4-O-sulfotransferases demonstrated using partially desulfated dermatan sulfate as an acceptor: implication of differential roles in dermatan sulfate biosynthesis. J Biol Chem 278:36115–36127.

Penc SF, Pomahac B, Winkler T, Dorschner RA, Eriksson E, Herndon M, Gallo RL. 1998. Dermatan sulfate released after injury is a potent promoter of fibroblast growth factor-2 function. J Biol Chem 273:28116–28121.

Scott JE. 1995. Extracellular matrix, supramolecular organisation and shape. J Anat 187(Pt 2):259–269.

Scott JE. 1996. Proteodermatan and proteokeratan sulfate (decorin, lumican/fibromodulin) proteins are horseshoe shaped. Implications for their interactions with collagen. Biochemistry 35:8795–8799.

Scott JE. 2003. Elasticity in extracellular matrix "shape modules" of tendon, cartilage, etc. A sliding proteoglycan-filament model. J Physiol 553(Pt 2):335–343.

Sonoda T, Kouno K. 2000. Two brothers with distal arthrogryposis, peculiar facial appearance, cleft palate, short stature, hydronephrosis, retentio testis, and normal intelligence: a new type of distal arthrogryposis? Am J Med Genet 91:280–285.

Steinmann B, Gitzelmann R, Vogel A, Grant ME, Harwood R, Sear CH. 1975. Ehlers-Danlos syndrome in two siblings with deficient lysyl hydroxylase activity in cultured skin fibroblasts but only mild hydroxylysine deficit in skin. Helv Paediatr Acta 30:255–274.

Steinmann B, Royce PM, Superti-Furga A. 2002. The Ehlers-Danlos syndrome. In: Royce PM, Stainmann B, editors. Connective tissue and heritable disorders. Hoboken, NJ: John Wiley & Sons Inc. p 431–523.

Sugahara K, Mikami T. 2007. Chondroitin/dermatan sulfate in the central nervous system. Curr Opin Struct Biol 17:536–545.

Tiedemann K, Olander B, Eklund E, Todorova L, Bengtsson M, Maccarana M, Westergren-Thorsson G, Malmstrom A. 2005. Regulation of the chondroitin/dermatan fine structure by transforming growth factor-beta1 through effects on polymer-modifying enzymes. Glycobiology 15:1277–1285.

Uyama T, Ishida M, Izumikawa T, Trybala E, Tufaro F, Bergstrom T, Sugahara K, Kitagawa H. 2006. Chondroitin 4-*O*-sulfotransferase-1 regulates E disaccharide expression of chondroitin sulfate required for herpes simplex virus infectivity. J Biol Chem 281:38668–38674.

Wenstrup RJ, Murad S, Pinnell SR. 1989. Ehlers-Danlos syndrome type VI: clinical manifestations of collagen lysyl hydroxylase deficiency. J Pediatr 115:405–409.

Yamagata T, Saito H, Habuchi O, Suzuki S. 1968. Purification and properties of bacterial chondroitinases and chondrosulfatases. J Biol Chem 243:1235–1523.

Yamaguchi Y, Mann DM, Ruoslahti E. 1990. Negative regulation of transforming growth factor-beta by the proteoglycan decorin. Nature 346:281–284.

Yasui H, Adachi Y, Minami T, Ishida T, Kato Y, Imai K. 2003. Combination therapy of DDAVP and conjugated estrogens for a recurrent large subcutaneous hematoma in Ehlers-Danlos syndrome. Am J Hematol 72:71–72.

Yoshida K, Arai M, Kohno Y, Maeyema KI, Myazono H, Kikuchi H, Morikawa K, Tawada A, Suzuki S. 1993. Activity of bacterial eliminases towards delmatan sulphates and dermatan sulphate proteoglycan. In: Scott JE, editor. Dermatan sulfate proteoglycans: chemistry, biology, chemical pathology. London: Portland Press. p 55–80.

Zawel L, Dai JL, Buckhaults P, Zhou S, Kinzler KW, Vogelstein B, Kern SE. 1998. Human Smad3 and Smad4 are sequence-specific transcription activators. Mol Cell 1:611–617.

Supp. Methods

PCR for haplotyping and Linkage analysis

For PCR amplification of microsatellite markers, we used 40 cycles of 94 °C for 30 sec, 55 °C for 30 sec and 72 °C for 30 sec in a total volume of 10 μl, containing 30 ng of genomic DNA as a template, 0.5 μM of each primer, 200 μM of each dNTP, 1 μl ExTaq buffer and 0.25 U ExTaq (Takara Bio, Inc., Otsu, Japan). Multipoint linkage analysis of aligned SNPs was performed using Allegro version 2 software (http://www.decode.com/software/allegro) on the assumption of an autosomal recessive model with full penetrance and a disease allele frequency of 0.001.

Expression vectors

For preparing mammalian expression vectors, the complete open reading frame of *CHST14* was amplified by PCR with KOD-Plus DNA polymerase (Toyobo, Osaka, Japan) using human genomic DNA as a template. The following primer set was used for amplification: 5′-**ACAAGTTTGTACAAAAAAGCAGGCTT**CATGTTCCCCCGCCCGCTG-3′ and 5′-**ACCACTTTGTACAAGAAAGCTGGGT**CTCACTGCTGACACGCCTCCTTG-3′ (bold characters indicate the linker sequence for BP recombination in the Gateway system provided by Invitrogen and the underlined sequences were added to fuse the PCR product in-frame with the N′-V5 tag). PCR products were cloned into pcDNA3.1/nV5-DEST (Invitrogen, Carlsbad, CA), which created N′-V5-tagged D4ST1. Quick change Site-Directed Mutagenesis kit (Stratagene, LaJolla, CA, USA) was used for generating cDNAs with each mutation. All the clones were confirmed by sequencing.

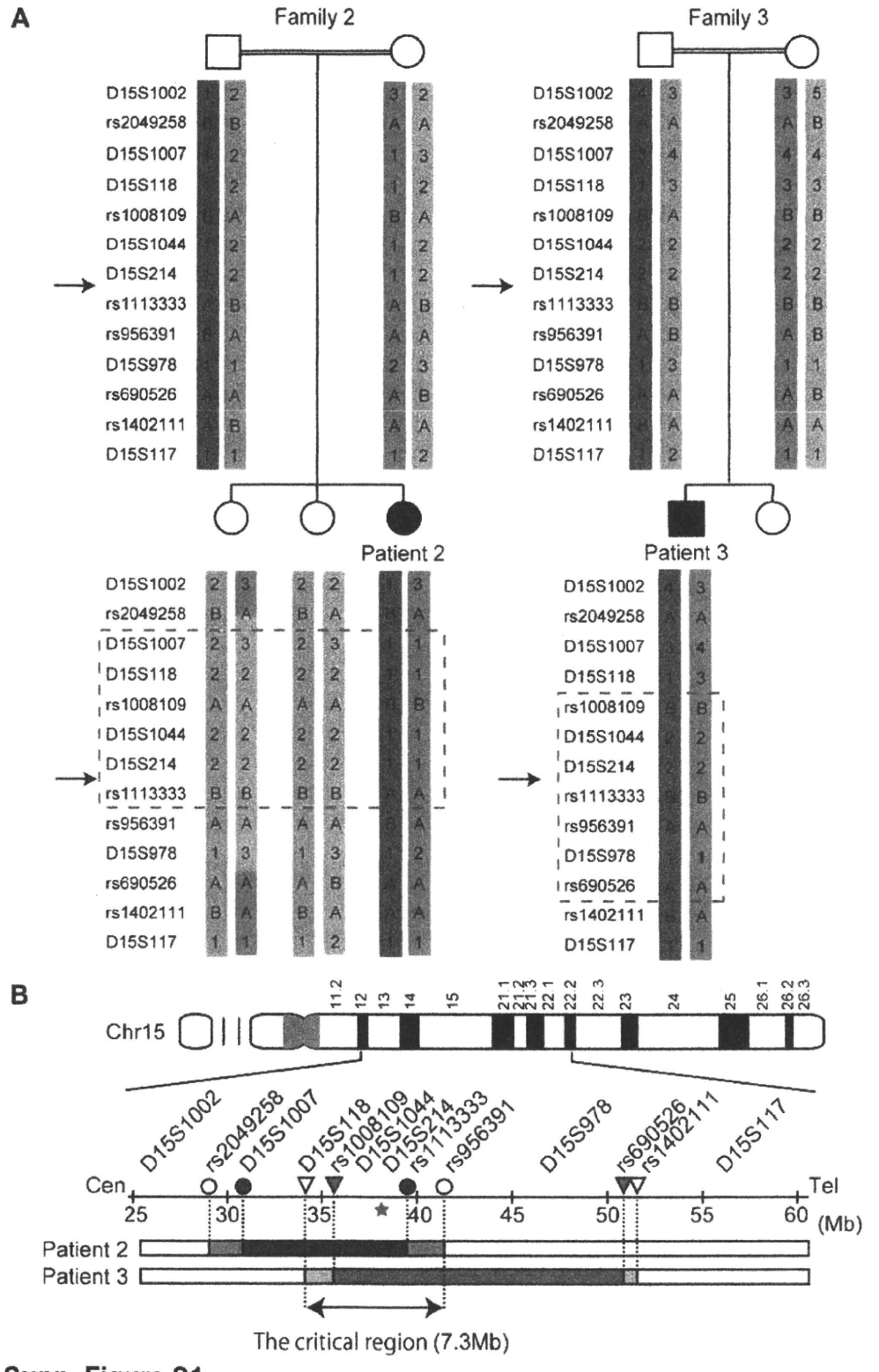

Supp. Figure S1

Supp. Figure S1. Disease locus and causative mutations in *CHST14*. **A:** Two consanguineous families (families 2 and 3) were subjected to homozygosity mapping. The red dashed box indicates the homozygous region in an affected proband in each pedigree. The arrow shows the position of the *CHST14* gene. Each chromosome is colored differently. **B:** The top depicts a schematic representation of human chromosome 15. In patient 2, blue and white circles indicate informative homozygous and heterozygous markers delimiting the disease locus, respectively. In patient 3, red and white triangles indicate informative homozygous and heterozygous markers, respectively. The common candidate region was narrowed down to 7.3 Mb (D15S118-rs956391).

from transgenes were approximately 300-fold those of endogenous mutant *CHST14* expression. **B:** The mRNA levels of *PAI1* and *SMAD7* were quantified by real-time PCR at 24 hr after TGF-β1 treatment. There were no statistically significant differences in the TGF-β1-induced expression levels of *PAI1* or *SMAD7* between the cells transfected with empty and *CHST14* vectors. **C:** Relative luciferase activity was measured using an SBE4-luc vector at 24 hr after TGF-β1 treatment. There were no statistically significant differences in TGF-β1-induced luciferase activity between the cells transfected with empty or *CHST14* vectors. **D:** The level of phosphorylated SMAD2 (p-SMAD2) protein was determined by western blot analysis at 30 min after TGF-β1 treatment. The upper panel shows the immunoblots stained with anti-p-SMAD2 and total SMAD2 antibodies with and without TGF-β1 stimulation in control and patient 1 fibroblasts. The middle panel shows immunoblots comparing wild-type and mutants for SMAD2 phosphorylation levels. The lower panel shows a densitometric analysis of p-SMAD2 relative to total SMAD2 and represents the mean ± s.e.m. (n = 3). There were no statistically significant differences in TGF-β1-induced SMAD2 phosphorylation between the cells transfected with empty or *CHST14* vectors.

Supp. Table S1. Total amount and disaccharide composition of CS/DS, DS, or CS chains in human fibroblasts[a]

CS/DS	pmol/mg protein (mol%)				
	Control 1	Control 2	Mother	Patient 1	Patient 3
ΔHexUA-GalNAc	272 (3.5)	279 (3.2)	427 (3.7)	317 (5.5)	606 (5.6)
ΔHexUA-GalNAc(6S)	1,804 (22.9)	1,178 (13.5)	1,832 (16.1)	1,854 (32.3)	3,492 (32.3)
ΔHexUA-GalNAc(4S)	5,597 (71.1)	7,177 (82.2)	8,961 (78.6)	3,399 (59.2)	6,393 (59.2)
ΔHexUA(2S)-GalNAc(6S)	193 (2.5)	96 (1.1)	187 (1.6)	170 (3.0)	315 (2.9)
ΔHexUA(2S)-GalNAc(4S)	N.D.	N.D.	N.D.	N.D.	N.D.
Total CS/DS disaccharide	7,866 (100)	8,730 (100)	11,407 (100)	5,740 (100)	10,805 (100)

DS	pmol/mg protein (mol%)				
	Control 1	Control 2	Mother	Patient 1	Patient 3
ΔHexUA-GalNAc	N.D.	N.D.	N.D.	N.D.	N.D.
ΔHexUA-GalNAc(6S)	N.D.	N.D.	N.D.	N.D.	N.D.
ΔHexUA-GalNAc(4S)	2,001 (100)	3,142 (100)	4,218 (100)	N.D.	N.D.
ΔHexUA(2S)-GalNAc(6S)	N.D.	N.D.	N.D.	N.D.	N.D.
ΔHexUA(2S)-GalNAc(4S)	N.D.	N.D.	N.D.	N.D.	N.D.
Total DS disaccharide	2,001 (100)	3,142 (100)	4,218 (100)	N.D.	N.D.

CS	pmol/mg protein (mol%)				
	Control 1	Control 2	Mother	Patient 1	Patient 3
ΔHexUA-GalNAc	74 (1.9)	97 (2.5)	41 (0.6)	23 (0.5)	30 (0.3)
ΔHexUA-GalNAc(6S)	1,521 (37.9)	967 (25.2)	1,940 (29.6)	1,572 (30.8)	2,990 (31.2)
ΔHexUA-GalNAc(4S)	2,420 (60.2)	2,768 (72.3)	4,570 (69.8)	3,513 (68.7)	6,561 (68.5)
ΔHexUA(2S)-GalNAc(6S)	N.D.	N.D.	N.D.	N.D.	N.D.
ΔHexUA(2S)-GalNAc(4S)	N.D.	N.D.	N.D.	N.D.	N.D.
Total CS disaccharide	4,015 (100)	3,832 (100)	6,551 (100)	5,108 (100)	9,581 (100)

[a]Total amount and disaccharide composition of CS/DS, DS, or CS chain in human fibroblasts was calculated based on the peak area in the chromatograms of the digests with CSase ABC, B, or AC, respectively.

N.D., not detected (<10 pmol/mg protein).

Journal of Human Genetics (2011) 56, 34–40

www.nature.com/jhg

ORIGINAL ARTICLE

A genome-wide association study identifies *RNF213* as the first Moyamoya disease gene

Fumiaki Kamada[1], Yoko Aoki[1], Ayumi Narisawa[1,2], Yu Abe[1], Shoko Komatsuzaki[1], Atsuo Kikuchi[3], Junko Kanno[1], Tetsuya Niihori[1], Masao Ono[4], Naoto Ishii[5], Yuji Owada[6], Miki Fujimura[2], Yoichi Mashimo[7], Yoichi Suzuki[7], Akira Hata[7], Shigeru Tsuchiya[3], Teiji Tominaga[2], Yoichi Matsubara[1] and Shigeo Kure[1,3]

Moyamoya disease (MMD) shows progressive cerebral angiopathy characterized by bilateral internal carotid artery stenosis and abnormal collateral vessels. Although ~15% of MMD cases are familial, the MMD gene(s) remain unknown. A genome-wide association study of 785 720 single-nucleotide polymorphisms (SNPs) was performed, comparing 72 Japanese MMD patients with 45 Japanese controls and resulting in a strong association of chromosome 17q25-ter with MMD risk. This result was further confirmed by a locus-specific association study using 335 SNPs in the 17q25-ter region. A single haplotype consisting of seven SNPs at the *RNF213* locus was tightly associated with MMD ($P=5.3\times10^{-10}$). *RNF213* encodes a really interesting new gene finger protein with an AAA ATPase domain and is abundantly expressed in spleen and leukocytes. An RNA *in situ* hybridization analysis of mouse tissues indicated that mature lymphocytes express higher levels of *Rnf213* mRNA than their immature counterparts. Mutational analysis of *RNF213* revealed a founder mutation, p.R4859K, in 95% of MMD families, 73% of non-familial MMD cases and 1.4% of controls; this mutation greatly increases the risk of MMD ($P=1.2\times10^{-43}$, odds ratio=190.8, 95% confidence interval=71.7–507.9). Three additional missense mutations were identified in the p.R4859K-negative patients. These results indicate that *RNF213* is the first identified susceptibility gene for MMD.
Journal of Human Genetics (2011) **56**, 34–40; doi:10.1038/jhg.2010.132; published online 4 November 2010

INTRODUCTION

'Moyamoya' is a Japanese expression for something hazy, such as a puff of cigarette smoke drifting in the air. In individuals with Moyamoya disease (MMD), there is a progressive stenosis of the internal carotid arteries; a fine network of collateral vessels, which resembles a puff of smoke on a cerebral angiogram, develops at the base of the brain (Figure 1a).[1,2] This steno-occlusive change can cause transient ischemic attacks and/or cerebral infarction, and rupture of the collateral vessels can cause intracranial hemorrhage. Children under 10 years of age account for nearly 50% of all MMD cases.[3]

The etiology of MMD remains unclear, although epidemiological studies suggest that bacterial or viral infection may be implicated in the development of the disease.[4] Growing attention has been paid to the upregulation of arteriogenesis and angiogenesis associated with MMD because chronic ischemia in other disease conditions is not always associated with a massive development of collateral vessels.[5,6] Several angiogenic growth factors are thought to have functions in the development of MMD.[7]

Several lines of evidence support the importance of genetic factors in susceptibility to MMD.[8] First, 10–15% of individuals with MMD have a family history of the disease.[9] Second, the concordance rate of MMD in monozygotic twins is as high as 80%.[10] Third, the prevalence of MMD is 10 times higher in East Asia, especially in Japan (6 per 100 000 population), than in Western countries.[3] Familial MMD may be inherited in an autosomal dominant fashion with low penetrance or in a polygenic manner.[11] Linkage studies of MMD families have revealed five candidate loci for an MMD gene: chromosomes 3p24–26,[12] 6q25,[13] 8q13–24,[10] 12p12–13[10] and 17q25.[14] However, no susceptibility gene for MMD has been identified to date.

We collected 20 familial cases of MMD to investigate linkage in the five putative MMD loci. However, a definitive result was not obtained for any of the loci. We then hypothesized that there might be a founder mutation among Japanese patients with MMD because the prevalence of MMD is unusually high in Japan.[15] Genome-wide and locus-specific association studies were performed and successfully identified a single gene, *RNF213*, linked to MMD. We report here a strong association between MMD onset and a founder mutation in *RNF213*, as well as the expression profiles of *RNF213*, in various tissues.

[1]Department of Medical Genetics, Tohoku University School of Medicine, Sendai, Japan; [2]Department of Neurosurgery, Tohoku University School of Medicine, Sendai, Japan; [3]Department of Pediatrics, Tohoku University School of Medicine, Sendai, Japan; [4]Department of Pathology, Tohoku University School of Medicine, Sendai, Japan; [5]Department of Microbiology and Immunology, Tohoku University School of Medicine, Sendai, Japan; [6]Department of Organ Anatomy, Yamaguchi University Graduate School of Medicine, Ube, Japan and [7]Department of Public Health, Graduate School of Medicine, Chiba University, Chiba, Japan
Correspondence: Dr S Kure, Department of Pediatrics, Tohoku University School of Medicine, 1-1 Seiryo-machi, Aoba-ku, Miyagi, Sendai 980-8574, Japan.
E-mail; kure@med.tohoku.ac.jp
Received 30 September 2010; accepted 1 October 2010; published online 4 November 2010

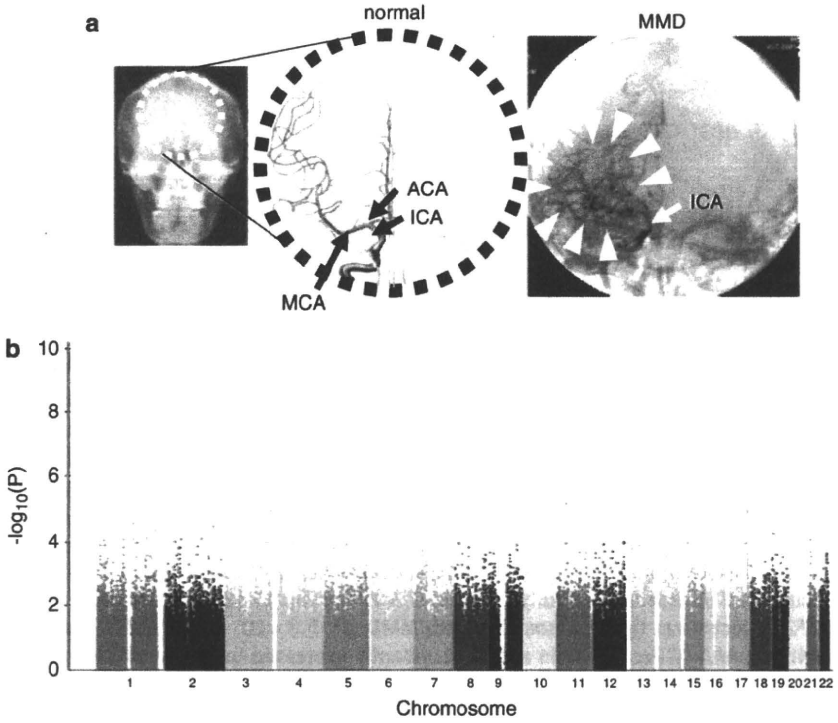

Figure 1 (**a**) Abnormal brain vessels in MMD. The dotted circle indicates the X-ray field of cerebral angiography (left panel). Normal structures of the right internal carotid artery (ICA), anterior cerebral artery (ACA) and middle cerebral artery (MCA) are illustrated (middle panel). The arrowheads indicate abnormal collateral vessels appearing like a puff of smoke in the angiogram of an individual with MMD (right panel). Note that ACA and MCA are barely visible, because of the occlusion of the terminal portion of the ICA. (**b**) Manhattan plot of the 785 720 SNPs used in the genome-wide association analysis of MMD patients. Note that the SNPs in the 17q25-ter region reach a significance of $P<10^{-8}$.

MATERIALS AND METHODS

Affected individuals

Genomic DNA was extracted from blood and/or saliva samples obtained from members of the families with MMD (Supplementary Figure 1), MMD patients with no family history and control subjects. All of the subjects were Japanese. MMD was diagnosed on the basis of guidelines established by the Research Committee on Spontaneous Occlusion of the Circle of Willis of the Ministry of Health and Welfare of Japan. This study was approved by the Ethics Committee of Tohoku University School of Medicine. Total RNA samples were purified from leukocytes using an RNeasy mini kit (Qiagen, Hilden, Germany) and used as templates for cDNA synthesis with an Oligo $(dT)_{20}$ primer and SuperScript II reverse transcriptase according to the manufacturer's instructions (Invitrogen, Carlsbad, CA, USA).

Linkage analysis

For the linkage analysis, DNA samples were genotyped for 36 microsatellite markers within five previously reported MMD loci using the ABI 373A DNA Sequencer (Applied Biosystems, Foster City, CA, USA). Pedigrees and haplotypes were constructed with the Cyrillic version 2.1 software (Oxfordshire, UK). Multipoint analyses were conducted using the GENEHUNTER 2 software (http://www.broadinstitute.org/ftp/distribution/software/genehunter/). Statistical analysis was performed with SPSS version 14.0J (SPSS, Tokyo, Japan).

Genome-wide and locus-specific association studies

A genome-wide association study was performed using a group of 72 MMD patients, which consisted of 64 patients without a family history of MMD and 8 probands of MMD families. The Illumina Human Omni-Quad 1 chip (Illumina, San Diego, CA, USA) was used for genotyping, and single-nucleotide polymorphisms (SNPs) with a genotyping completion rate of 100% were used for further statistical analysis (785 720 out of 1 140 419 SNPs). Genotyping data from 45 healthy Japanese controls were obtained from the database at the International HapMap Project web site. The 785 720 SNPs were statistically analyzed using the PLINK software (http://pngu.mgh.harvard.edu/~purcell/plink/index.shtml). For a locus-specific association study, we used 63 DNA samples consisting of 58 non-familial MMD patients and 5 probands of MMD families. A total of 384 SNPs within chromosome 17q25-ter were genotyped (Supplementary Table 1), using the GoldenGate Assay and a custom SNP chip (Illumina). Genotyping data for 45 healthy Japanese were used as a control. Case–control single-marker analysis, haplotype frequency estimation and significance testing of differences in haplotype frequency were performed using the Haploview version 3.32 program (http://www.broad.mit.edu/mpg/haploview/).

Mutation detection

Mutational analyses of *RNF213* and *FLJ35220* were performed by PCR amplification of each coding exon and putative promoter regions, followed by direct sequencing. Genomic sequence data for the two genes were obtained from the National Center for Biotechnology Information web site (http://www.ncbi.nlm.nih.gov/) for design of exon-specific PCR primers. *RNF213* cDNA fragments were amplified from leukocyte mRNA for sequencing analysis. Sequencing of the PCR products was performed with the ABI BigDye Terminator Cycle Sequencing Reaction Kit using the ABI 310 Genetic Analyzer. Identified base changes were screened in control subjects. Statistical difference of the carrier frequency of each base change was estimated by Fisher's exact test (the MMD group vs the control group).

Quantitative PCR

MTC Multiple Tissue cDNA Panels (Clontech Laboratory, Madison, WI, USA) were the source of cDNAs from human cell lines, adult and fetal tissues. Mononuclear cells and polymorphonuclear cells were isolated from the fresh peripheral blood of healthy human adults using Polymorphprep (Cosmo Bio,

Carlsbad, CA, USA). T and B cells were isolated from the fresh peripheral blood of healthy human adults using the autoMACS separator (Militeny Biotec, Bergisch Gladbach, Germany). Total RNA was isolated from these cells with the RNeasy Mini Kit (Qiagen) following the manufacturer's instructions. We reverse transcribed 100 ng samples of total RNA into cDNAs using the High Capacity cDNA Reverse Transcription Kit (Applied Biosystems). Quantitative PCRs were performed in a final volume of 20 μl using the FastStart TaqMan Probe Master (Rox) (Roche, Madison, WI, USA), 5 μl of cDNA, 10 μM of *RNF*- or *GAPDH*-specific primers and 10 μM of probes (Universal ProbeLibrary Probe #80 for *RNF213* and Roche Probe #60 for *GAPDH*). All reactions were performed in triplicate using the ABI 7500 Real-Time PCR system (Applied Biosystems). Cycling conditions were 2 min at 50°C and 10 min at 95°C, followed by 40 cycles of 15 s at 95°C and 60 s at 60°C. Real-time PCR data were analyzed by the SDS version 1.2.1 software (Applied Biosystems). We evaluated the relative level of *RNF213* mRNA by determining the C_T value, the PCR cycle at which the reporter fluorescence exceeded the signal baseline. *GAPDH* mRNA was used as an internal reference for normalization of the quantitative expression values.

Multiplex PCR

MTC Multiple Tissue cDNA Panels (Clontech) were the source of human cell lines and cDNAs from human adult and fetal tissues. Multiplex PCRs were performed in a final volume of 20 μl using the Multiplex PCR Master Mix (Qiagen), 2 μl of cDNA, a 2 μM concentration of *RNF213* and a 10 μM concentration of *GAPDH*-specific primers. The samples were separated on a 2% agarose gel stained with ethidium bromide. Cycling conditions were 15 min at 94°C, followed by 30 cycles of 30 s at 94 °C, 30 s at 57 °C and 30 s at 72 °C. For normalization of the expression levels, we used *GAPDH* as an internal reference for each sample.

In situ hybridization (ISH) analysis

Paraffin-embedded blocks and sections of mouse tissues for ISH were obtained from Genostaff (Tokyo, Japan). The mouse tissues were dissected, fixed with Tissue Fixative (Genostaff), embedded in paraffin by proprietary procedures (Genostaff) and sectioned at 6 μm. To generate anti-sense and sense RNA probes, a 521-bp DNA fragment corresponding to nucleotide positions 470–990 of mouse *Rnf213* (BC038025) was subcloned into the pGEM-T Easy vector (Promega, Madison, WI, USA). Hybridization was performed with digoxigenin-labeled RNA probes at concentrations of 300 ng ml^{-1} in Probe Diluent-1 (Genostaff) at 60 °C for 16 h. Coloring reactions were performed with NBT/BCIP solution (Sigma-Aldrich, St Louis, MO, USA). The sections were counterstained with Kernechtrot stain solution (Mutoh, Tokyo, Japan), dehydrated and mounted with Malinol (Mutoh). For observation of *Rnf213* expression in activated lymphocytes, 10-week-old Balb/c mice were intraperitoneally injected with 100 μg of keyhole limpet hemocyanin and incomplete adjuvant and sacrificed in 2 weeks. The spleen of the mice was removed for Hematoxylin–eosin staining and ISH analyses.

RESULTS

Using 20 Japanese MMD families, we reevaluated the linkage mapped previously to five putative MMD loci. No locus with significant linkage, Lod score >3.0 or NPL score >4.0 was confirmed (Supplementary Figure 2). We conducted a genome-wide association study of 72 Japanese MMD cases. Single-marker allelic tests comparing the 72 MMD cases and 45 controls were performed for 785 720 SNPs using χ^2 statistics. These tests identified a single locus with a strong association with MMD ($P<10^{-8}$) on chromosome 17q25-ter (Figure 1b), which is in line with the latest mapping data of a MMD locus.[16] The SNP markers with $P<10^{-6}$ are listed in Table 1. To confirm this observation, we performed a locus-specific association study. A total of 384 SNP markers (Supplementary Table 1) were selected within the chromosome 17q25-ter region and genotyped in a set of 63 MMD cases and 45 controls. The SNP markers demonstrating a high association with MMD ($P<10^{-6}$) were clustered in a 151-kb region from base position 75 851 399–76 003 020 (SNP No.116–136 in

Table 1 A genome-wide association study of Japanese MMD patients and controls

	SNP	Chromosome	Base position	Gene	Risk allele/ non-risk allele	Risk allele frequency in MMD	Risk allele frequency in controls	χ^2	P-value	Odds ratio	95% confidence interval	
											Lower	Upper
1	rs11870849	17	76 025 668	*RNF213*	T/C	0.4792	0.1111	33.55	6.95E-09	7.36	3.532	15.34
2	rs6565681	17	75 963 089	*RNF213*	A/G	0.7361	0.3667	31.35	2.16E-08	4.819	2.733	8.489
3	rs7216493	17	75 941 953	*RNF213*	G/A	0.75	0.3889	30.39	3.53E-08	4.715	2.673	8.313
4	rs7217421	17	75 850 055	*RNF213*	A/G	0.6667	0.3	29.86	4.64E-08	4.666	2.642	8.237
5	rs12449863	17	75 857 806	*RNF213*	C/T	0.6667	0.3	29.86	4.64E-08	4.666	2.642	8.237
6	rs4890009	17	75 926 103	*RNF213*	G/A	0.8819	0.5778	28.5	9.38E-08	5.459	2.831	10.527
7	SNP17-75933731	17	75 933 731	*RNF213*	G/A	0.8819	0.5778	28.5	9.38E-08	5.458	2.831	10.527
8	rs7219131	17	75 867 365	*RNF213*	T/C	0.6667	0.3111	28.11	1.15E-07	4.429	2.517	7.794
9	rs6565677	17	75 932 037	*RNF213*	T/C	0.7431	0.3977	27.43	1.63E-07	4.378	2.483	7.722
10	rs4889848	17	75 969 256	*RNF213*	C/T	0.75	0.4111	26.99	2.05E-07	4.297	2.444	7.889
11	rs7224239	17	75 969 771	*RNF213*	A/G	0.8681	0.5667	26.99	2.05E-07	5.03	2.659	9.529

Abbreviations: MMD, moyamoya disease; SNP, single-nucleotide polymorphism.A genome-wide association study testing 1 140 419 SNPs on the Human Omni-Quad 1chip (Illumina, San Diego, CA, USA) was performed in 72 Japanese MMD cases. Single-marker allelic tests between the cases and controls were performed using χ^2 statistics for all markers. This table lists the 11 SNP markers with a significance of $P<10^{-6}$.

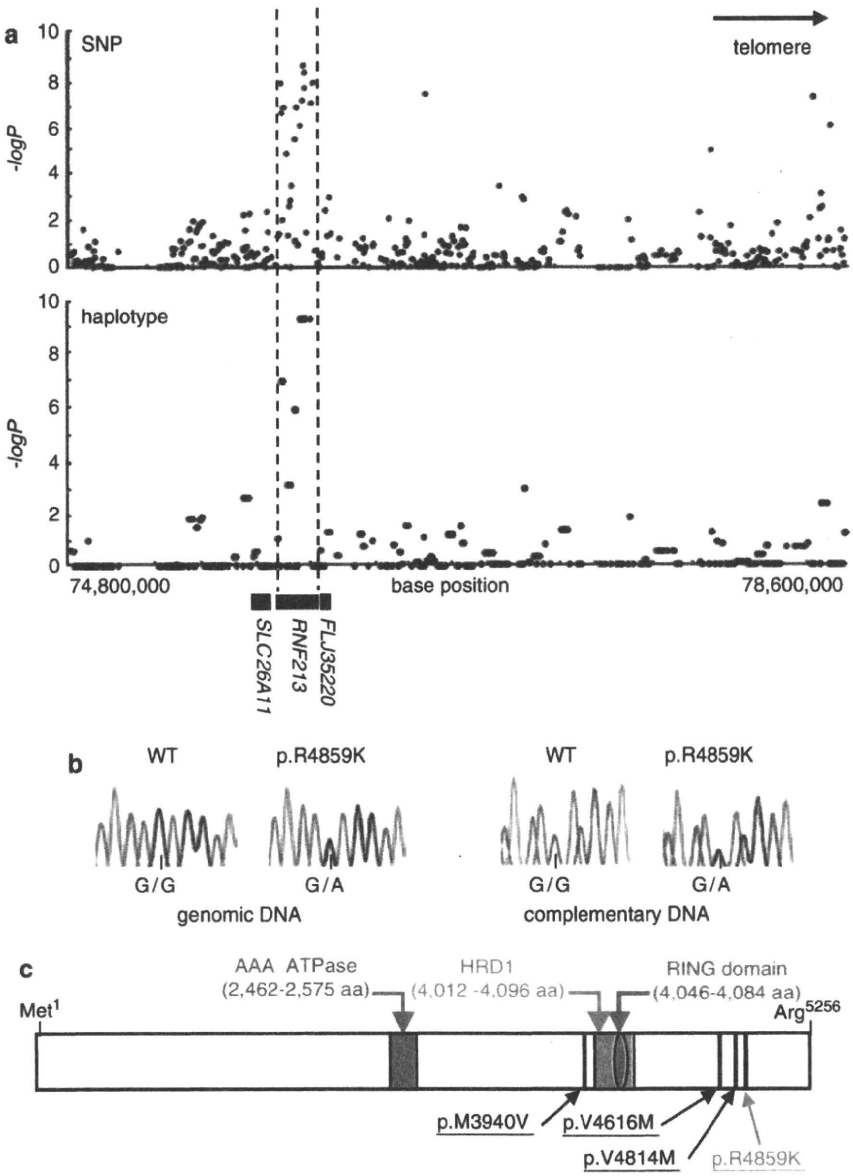

Figure 2 (**a**) Association analysis of 63 non-familial MMD cases and 45 control subjects. Statistical significance was evaluated by the χ^2-test. SNP markers with a strong association with MMD ($P<10^{-6}$) clustered in a 161-kb region (base position 75851399–76012838) indicated by two dotted lines (upper panel), which included the entire region of *RNF213* (lower panel). Haplotype analysis revealed a strong association ($P=5.3\times10^{-10}$) between MMD and a single haplotype located within *RNF213*. (**b**) Sequencing chromatograms of the identified MMD mutations. The left panel shows the sequences of an unaffected individual and a carrier of a p.R4859K heterozygous mutation. The right panel indicates the sequencing chromatograms of the leukocyte cDNA obtained from an unaffected individual and an individual with MMD who carries the p.R4859K mutation. Note that both wild-type and mutant alleles were expressed in leukocytes. (**c**) The structure of the RNF213 protein. The RNF213 protein contains three characteristic structures, the AAA-superfamily ATPase motif, the RING motif and the HMG-CoA reductase degradation motif. The positions of four mutations identified in MMD patients are underlined, including one prevalent mutation (red) and three private mutations (black).

Supplementary Table 1); this entire region was within the *RNF213* locus (Figure 2a). A single haplotype determined by seven SNPs (SNP Nos.130–136 in Supplementary Table 1) that resided in the 3′ region of *RNF213* was strongly associated with MMD onset ($P=5.3\times10^{-10}$). Analysis of the linkage disequilibrium block indicated that this haplotype was not in complete linkage disequilibrium with any other haplotype in this region (Supplementary Figure 3). These results strongly suggest that a founder mutation may exist in the 3′ part of *RNF213*.

Mutational analysis of the entire coding and promoter regions of *RNF213* and *FLJ35220*, a gene 3′ adjacent to *RNF213*, revealed that 19 of the 20 MMD families shared the same single base substitution, c.14576G>A, in exon 60 of *RNF213* (Figure 2b and Table 2). This nucleotide change causes an amino-acid substitution from arginine^{4859} to lysine^{4859} (p.R4859K). The p.R4859K mutation was identified in 46 of 63 non-familial MMD cases (73%), including 45 heterozygotes and a single homozygote (Table 3). Both the wild-type and the p.R4859K mutant alleles were co-expressed in leukocytes

Table 2 Nucleotide changes with amino-acid substitutions identified in the sequencing analysis of *RNF213* and *FLJ35220*

			Genotype (allele)				
Gene	*Exon*	*Nucleotide change[a] (amino-acid substitution)*	*Non-familial cases*	*Control subjects*	*P-value[b]*	*χ^2 (df=1)[c]*	*Odds ratio (95% CI)*
RNF213	29	c.7809C>A (p.D2603E)	2/63 (2/126)	15/381 (15/762)	0.77	0.09	0.80 (0.2–3.6)
RNF213	41	c.11818A>G (p.M3940V)	1/63 (1/126)	0/388 (0/776)	0.01	6.17	ND
RNF213	41	c.11891A>G (p.E3964G)	4/63 (4/126)	3/55 (4/110)	0.84	0.04	1.2 (0.3–5.5)
RNF213	52	c.13342G>A (p.A4448T)	4/63 (4/126)	2/53 (2/106)	0.53	0.39	1.7 (0.3–9.8)
RNF213	56	c.13846G>A (p.V4616M)	1/63 (1/126)	0/388 (0/776)	0.01	6.17	ND
RNF213	59	c.14440G>A (p.V4814M)	1/63 (1/126)	0/388 (0/776)	0.01	6.17	ND
RNF213	60	c.14576G>A (p.R4859K)	46/63 (47/126)	6/429 (6/858)	1.2×10^{-43}	298.1	190.8 (71.7–507.9)
FLJ35220		None					

Abbreviations: ND, not determined; SNP, single-nucleotide polymorphism.
[a]Nucleotide numbers of *RNF213* cDNA are counted from the A of the ATG initiator methionine codon (NCBI Reference sequence, NP_065965.4).
[b]*P*-values were calculated by Fisher's exact test.
[c]Genotypic distribution (carrier of the polymorphism vs non-carrier).

Table 3 Association of the p.R4859K (c.14576G>A) mutation with MMD

		Genotype		
	Total	*wt/wt (%)*	*wt/p.R4859K (%)*	*p.R4859K/p.R4859K (%)[d]*
Members of 19 MMD families[a]				
Affected	42	0	39 (92.9)	3 (7.1)
Not affected	28	15 (53.6)	13 (46.4)	0
Individuals without a family history of MMD[b,c]				
Affected	63	17 (27.0)	45 (71.4)	1 (1.6)
Not affected	429	423 (98.6)	6 (1.4)	0

Abbreviations: MMD, moyamoya disease.
[a]Entire distribution, $\chi^2=29.4$, $P=4.2\times10^{-7}$.
[b]Entire distribution, $\chi^2=298.2$, $P=1.8\times10^{-65}$.
[c]Genotypic distribution (p.R4859K carrier vs non-carrier), $\chi^2=298.1$, $P=1.2\times10^{-43}$, odds ratio=190.8 (95% CI=71.7–507.9).
[d]The age of onset and initial symptoms of the four homozygotes were comparable to those of the 84 heterozygous patients.

in three patients heterozygous for the p.R4859K mutation (Figure 2b), excluding the possible instability of the mutant *RNF213* mRNA. Additional missense mutations, p.M3940V, p.V4616M and p.V4814M, were detected in three non-familial MMD cases without the p.R4859K mutation (Figure 2c). These mutations were not found in 388 control subjects and were detected in only one patient, suggesting that they were private mutations (Table 2). No copy number variation or mutation was identified in the *RNF213* locus of 12 MMD patients using comparative genome hybridization microarray analysis (Supplementary Figure 4). In total, 6 of the 429 control subjects (1.4%) were found to be heterozygous carriers of p.R4859K. Therefore, we concluded that the p.R4859K mutation increases the risk of MMD by a remarkably high amount (odds ratio=190.8 (95% confidence interval=71.7–507.9), $P=1.2\times10^{-43}$) (Table 3). It was recently reported that an SNP (ss161110142) in the promoter region of *RPTOR*, which is located ~150 kb downstream from *RNF213*, was associated with MMD.[17] Genotyping of the SNP in *RPTOR* showed that the *RNF213* p.R4859K mutation was more strongly associated with MMD than ss161110142 (Supplementary Figure 1).

RNF213 encodes a protein with 5256 amino acids harboring a RING (really interesting new gene) finger motif, suggesting that it functions as an E3 ubiquitin ligase (Figure 2c). It also has an AAA ATPase domain, which is characteristic of energy-dependent unfoldases.[18] To our knowledge, RNF213 is the first RING finger protein known to contain an AAA ATPase domain. The expression profile of *RNF213* has not been previously fully characterized. We performed a quantitative reverse transcription PCR analysis in various human tissues and cells. *RNF213* mRNA was highly expressed in immune tissues, such as spleen and leukocytes (Figure 3a and Supplementary Figure 5). Expression of *RNF213* was detected in fractions of both polymorphonuclear cells and mononuclear cells and was found in both B and T cell fractions (Supplementary Figure 6). A low but significant expression of *RNF213* was also observed in human umbilical vein endothelial cells and human pulmonary artery smooth muscle cells. Cellular expression was not enhanced in tumor cell lines, compared with leukocytes. In human fetal tissues, the highest expression was observed in leukocytes and the thymus (Supplementary Figure 6E). The expression of *RNF213* was surprisingly low in both adult and fetal brains. Overall, *RNF213* was ubiquitously expressed, and the highest expression was observed in immune tissues.

We studied the cellular expression of *Rnf213* in mice. The ISH analysis of spleen showed that *Rnf213* mRNA was present in small mononuclear cells, which were mainly localized in the white pulps (Figures 3b–g). The ISH signals were also detected in the primary follicles in the lymph node and in thymocytes in the medulla of the thymus (Supplementary Figure 7). To study *Rnf213* expression in activated lymphocytes we immunized mice with keyhole limpet hemocyanin, and examined *Rnf213* mRNA in spleen by ISH analysis. Primary immunization with keyhole limpet hemocyanin antigen revealed that the expression of *Rnf213* in the secondary follicle is as high as in the primary follicle in the lymph node (Supplementary Figure 8). In an E16.5 mouse embryo, expression was observed in the medulla of the thymus and in the cells around the mucous palatine glands (Supplementary Figure 9). These findings suggest that mature lymphocytes in a static state express *Rnf213* mRNA at a higher level than do their immature counterparts.

DISCUSSION

We identified a susceptibility locus for MMD by genome-wide and locus-specific association studies. Further sequencing analysis revealed a founder missense mutation in *RNF213*, p.R4859K, which was tightly associated with MMD onset. Identification of a founder mutation in individuals with MMD would resolve the following recurrent

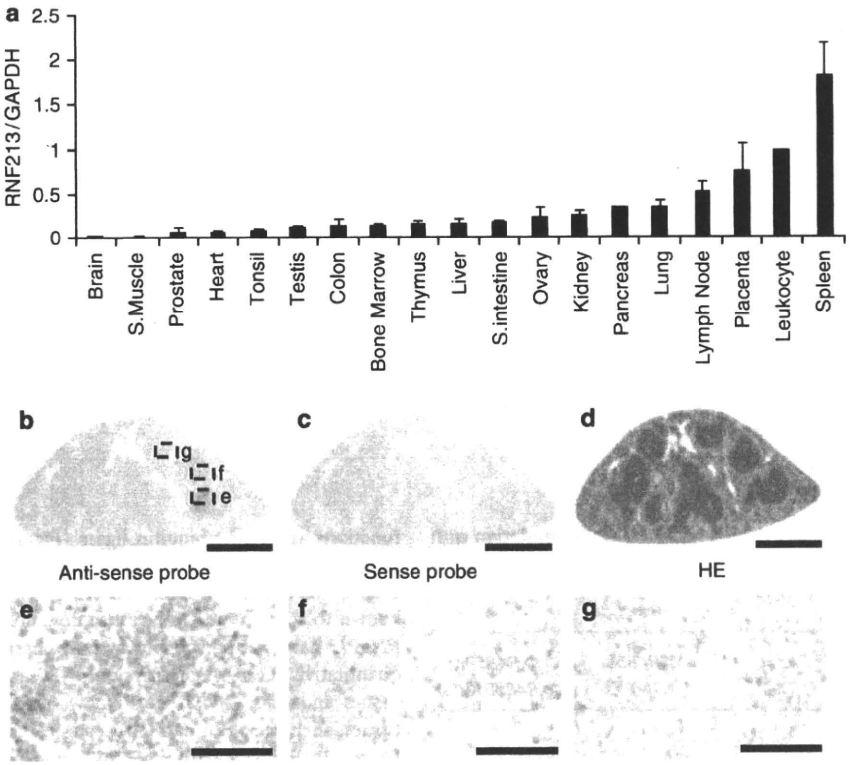

Figure 3 Expression of human RNF213 and murine Rnf213. (**a**) RT-PCR analysis of RNF213 mRNA in various human tissues. The expression levels of *RNF213* mRNA in various adult human tissues were evaluated by quantitative PCR using *GAPDH* mRNA as a control. The signal ratio of *RNF213* mRNA to *GAPDH* mRNA in each sample is shown on the vertical axis. (**b–g**) *In situ* hybridization (ISH) analysis of Rnf213 mRNA in mouse spleen. Specific signals for *Rnf213* mRNA were detected by ISH analysis with the anti-sense probe (**b**) but not with the sense probe (**c**). Hematoxylin–eosin staining of the mouse spleen (**d**). Signals for the *Rnf213* mRNA were observed in small mononuclear cells, which were mainly localized in the white pulps (dotted square, **e**) and partially distributed in the red pulps (dotted squares, **f** and **g**). Panels e, f and g show the high-magnification images of the corresponding fields in panel b. Scale bars, 1 mm (**b–d**) and 50 μm (**e–g**).

questions:[2,19] (i) why is MMD more prevalent in East Asia than in Western countries? The carrier frequency of p.R4859K in Japan is 1/72 (Table 2). In contrast, we found no p.R4859K carrier in 400 Caucasian controls (data not shown). Furthermore, no mutation was identified in five Caucasian patients with MMD after the full sequencing of *RNF213*. These results suggest that the genetic background of MMD in Asian populations is distinct from that in Western populations and that the low incidence of MMD in Western countries may be attributable to a lack of the founder *RNF213* mutation. (ii) Is unilateral involvement a subtype of MMD or a different disease?[2] We collected DNA samples from six patients with unilateral involvement and found a p.R4859K mutation in four of them (data not shown), suggesting that bilateral and unilateral MMD share a genetic background. (iii) Is pre-symptomatic diagnosis of MMD possible? In the present study, MMD never developed in the 15 mutation-negative family members in the 19 MMD families with the p.R4859K mutation (Table 3 and Supplementary Figure 1), suggesting the feasibility of presymptomatic diagnosis or exclusion by genetic testing.

How the mutant RNF213 protein causes MMD remains to be elucidated. The expression of *RNF213* was more abundant in a subset of leukocytes than in the brain, suggesting that blood cells have a function in the etiology of MMD. This observation agrees with a previous report that MMD patients have systemic angiopathy.[20] Recent studies have suggested that the postnatal vasculature can form through vasculogenesis, a process by which endothelial progenitor cell are recruited from the splenic pool and differentiate into mature endothelial cells.[21] Levels of endothelial progenitor cells in the peripheral blood are increased in MMD patients.[22] *RNF213* may be expressed in splenic endothelial progenitor cells and mutant *RNF213* might dysregulate the function of the endothelial progenitor cells. Further research is necessary to elucidate the role of *RNF213* in the etiology of MMD.

CONFLICT OF INTEREST

The authors declare no conflict of interest.

ACKNOWLEDGEMENTS

We thank all of the patients and their families for participating in this study. We also thank Dr Hidetoshi Ikeda at the Department of Neurosurgery, Tohoku University School of Medicine and Drs Toshiaki Hayashi and Reizo Shirane at the Department of Neurosurgery, Miyagi Children's Hospital, Sendai, Japan for patient recruitment. We are grateful to Ms Kumi Kato for technical assistance. This study was supported by grants from the Ministry of Education, Culture, Sports, Science and Technology, Japan and by the Research Committee on Moyamoya Disease of the Ministry of Health, Labor and Welfare, Japan.

1 Suzuki, J. & Takaku, A. Cerebrovascular 'moyamoya' disease. Disease showing abnormal net-like vessels in base of brain. *Arch. Neurol.* **20,** 288–299 (1969).
2 Suzuki, J. *Moyamoya Disease* (Springer-Verlag: Berlin, 1983).
3 Oki, K., Hoshino, H. & Suzuki, N. In: *Moyamoya Disease Update*, (eds Cho B.K., Tominaga T.) 29–34 (Springer: New York, 2010).
4 Phi, J. H., Kim, S. K., Wang, K. C. & Cho, B. K. In: *Moyamoya Disease Update*, (eds Cho B.K., Tominaga T). 82–86, (Springer: New York, 2010).
5 Yoshihara, T., Taguchi, A., Matsuyama, T., Shimizu, Y., Kikuchi-Taura, A., Soma, T. *et al.* Increase in circulating CD34-positive cells in patients with angiographic evidence of moyamoya-like vessels. *J. Cereb. Blood Flow Metab.* **28,** 1086–1089 (2008).
6 Achrol, A. S., Guzman, R., Lee, M. & Steinberg, G. K. Pathophysiology and genetic factors in moyamoya disease. *Neurosurg. Focus.* **26,** E4 (2009).
7 Scott, R. M. & Smith, E. R. Moyamoya disease and moyamoya syndrome.. *N. Engl. J. Med.* **360,** 1226–1237 (2009).
8 Kure, S. In: *Moyamoya Disease Update* (eds Cho B.K., Tominaga T.) 41–45 (Springer: Tokyo, 2010).
9 Kuriyama, S., Kusaka, Y., Fujimura, M., Wakai, K., Tamakoshi, A., Hashimoto, S. *et al.* Prevalence and clinicoepidemiological features of moyamoya disease in Japan: findings from a nationwide epidemiological survey. *Stroke.* **39,** 42–47 (2008).
10 Sakurai, K., Horiuchi, Y., Ikeda, H., Ikezaki, K., Yoshimoto, T., Fukui, M. *et al.* A novel susceptibility locus for moyamoya disease on chromosome 8q23. *J. Hum. Genet.* **49,** 278–281 (2004).
11 Nanba, R., Kuroda, S., Tada, M., Ishikawa, T., Houkin, K. & Iwasaki, Y. Clinical features of familial moyamoya disease. *Childs. Nerv. Syst.* **22,** 258–262 (2006).
12 Ikeda, H., Sasaki, T., Yoshimoto, T., Fukui, M. & Arinami, T. Mapping of a familial moyamoya disease gene to chromosome 3p24.2-p26. *Am. J. Hum. Genet.* **64,** 533–537 (1999).
13 Inoue, T. K., Ikezaki, K., Sasazuki, T., Matsushima, T. & Fukui, M. Linkage analysis of moyamoya disease on chromosome 6. *J. Child. Neurol.* **15,** 179–182 (2000).
14 Yamauchi, T., Tada, M., Houkin, K., Tanaka, T., Nakamura, Y., Kuroda, S. *et al.* Linkage of familial moyamoya disease (spontaneous occlusion of the circle of Willis) to chromosome 17q25.. *Stroke.* **31,** 930–935 (2000).
15 Wakai, K., Tamakoshi, A., Ikezaki, K., Fukui, M., Kawamura, T., Aoki, R. *et al.* Epidemiological features of moyamoya disease in Japan: findings from a nationwide survey. *Clin. Neurol. Neurosurg.* **99**(Suppl 2), S1–S5 (1997).
16 Mineharu, Y., Liu, W., Inoue, K., Matsuura, N., Inoue, S., Takenaka, K. *et al.* Autosomal dominant moyamoya disease maps to chromosome 17q25.3. *Neurology.* **70,** 2357–2363 (2008).
17 Liu, W., Hashikata, H., Inoue, K., Matsuura, N., Mineharu, Y., Kobayashi, H. *et al.* A rare Asian founder polymorphism of Raptor may explain the high prevalence of Moyamoya disease among East Asians and its low prevalence among Caucasians. *Environ. Health. Prev. Med.* **15,** 94–104 (2010).
18 Lupas, A. N. & Martin, J. AAA proteins.. *Curr. Opin. Struct. Biol.* **12,** 746–753 (2002).
19 Ikezaki, K. In: *Moyamoya disease* (eds Ikezaki K., Loftus C. M.) 43–75 (Thieme: New York, 2001).
20 Ikeda, E. Systemic vascular changes in spontaneous occlusion of the circle of Willis. *Stroke.* **22,** 1358–1362 (1991).
21 Zampetaki, A., Kirton, J. P. & Xu, Q. Vascular repair by endothelial progenitor cells. *Cardiovasc. Res.* **78,** 413–421 (2008).
22 Rafat, N., Beck, G., Pena-Tapia, P. G., Schmiedek, P. & Vajkoczy, P. Increased levels of circulating endothelial progenitor cells in patients with Moyamoya disease. *Stroke.* **40,** 432–438 (2009).

Supplementary Information accompanies the paper on Journal of Human Genetics website (http://www.nature.com/jhg)